ON LONGITUDINAL COMPRESSIVE FAILURE OF CFRP: from unidirectional to woven, and from virgin to recycled

S. T. Pinho[1*], R. Gutkin[1], S. Pimenta[1], N. V. De Carvalho[1], P. Robinson[1]

[1] *Dept. of Aeronautics, Imperial College London, South Kensington, London, SW7 2AZ, UK.*

***** *silvestre.pinho@imperial.ac.uk*

Abstract

Modelling the longitudinal compressive failure of carbon fibre reinforced composites has been attempted for decades. Despite many developments, no single model has surfaced as providing simultaneously a definitive explanation for the micromechanics of failure as well as validated predictions for a generic stress state. This paper explores the reasons for this, by presenting experimental data (including scanning electron microscopic observations of loaded kink bands during propagation, and brittle shear fracture at 45° to the fibres) and reviewing previously proposed micromechanical analytical and numerical models. The paper focuses mainly on virgin unidirectional composites, but studies for woven and recycled composites are also presented, highlighting similarities and differences between these cases. It is found that, while kink-band formation (also referred to in the literature as micro-buckling) is predominant in unidirectional composites under longitudinal compression, another failure mode related to the failure of the fibres can be observed experimentally. It is also shown that the micromechanics of the failure process observed in unidirectional composites is similar to that in other fibre architectures, hence encouraging the adaptation and application of models developed for the former to the latter.

Keywords: kink band; composite; fracture; unidirectional; woven; recycled

1. Introduction

Longitudinal compressive failure has been a topic of research for several decades due to its significance in structural design. Different models have been proposed, based on microbuckling of the fibres [1] and on fibre kinking [2] (Figure 1). Key developments to these theories were later proposed for instance in [3-5]; Figure 1c shows failure predictions for longitudinal loading (σ_{11}) combined with in-plane shear (τ_{12}) for several models (polynomial, e.g. Tsai-Wu and maximum stress; physically-based, e.g. Puck and LaRC05), see [7] for a discussion.

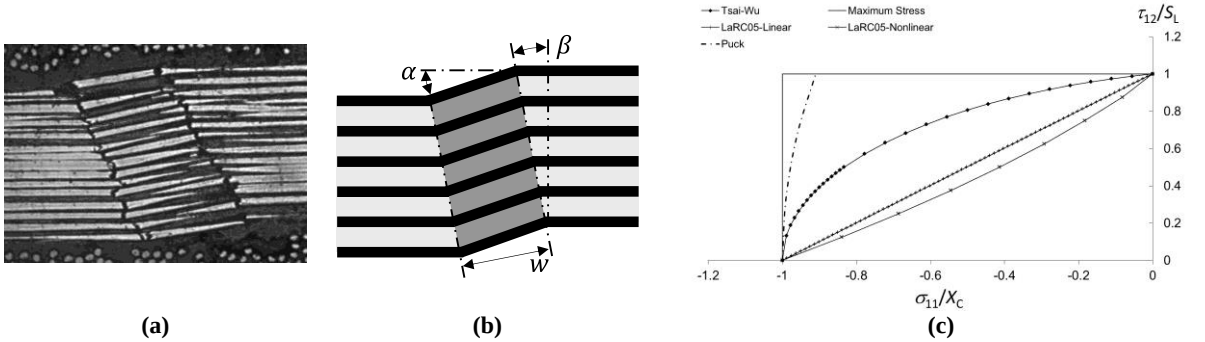

(a) **(b)** **(c)**

Figure 1: (a) micrograph of a kink band; (b) typical kink-band geometrical parameters (*α*:fibre orientation; *β*:band orientation; *w*: band width) [6]; (c) failure envelope under combined longitudinal compression and shear—the longitudinal and shear stresses are non-dimensionalised by their respective strength X_c and S_L [7].

Pinho ST, Gutkin R, Pimenta S, De Carvalho NV, Robinson P (2012). On longitudinal compressive failure of carbon-fibre-reinforced polymer: from unidirectional to woven, and from virgin to recycled. *Royal Society of London. Philosophical Transactions A. Mathematical, Physical and Engineering Sciences* 370, 1871-1895. DOI: 10.1098/rsta.2011.0429

The experimental, numerical and analytical results presented in this paper highlight the physical processes underlying longitudinal compressive failure for a range of composites, focusing mainly on unidirectional (UD) composites (section 2). Section 2.1 introduces experimental observations and Finite Element (FE) micromechanical modelling results which support the development of a model for fibre kinking under pure longitudinal compression (also presented). Section 2.2 uses a similar approach to analyse kink-band formation for longitudinal compression superposed with in-plane shear. The two approaches complement each other with the first one based on a plasticity model, suitable for ductile resins, while the second one is based on finite fracture mechanics principles more suited to brittle resins. Section 2.3 finally investigates a different failure mode under longitudinal compression: shear-driven fibre compressive failure. Similar work for woven composites is presented in section 3 and for recycled composites in section 4. The relation between the compressive failure mechanisms is discussed in section 5 and conclusions are drawn in section 6.

2. The physics of fibre kinking in UD plies

2.1. Pure longitudinal compression

2.1.1. Experimental observations

Using Scanning Electron Microscopy (SEM), observations of loaded kink bands during propagation (Figure 2, see also [8]) reveal how their formation is related to the development of microcracks in the matrix (label "m" in Figure 2c) which can coalesce in splits (label "c" in Figure 2c), and with fibre failure only appearing relatively late in the process. Carbon fibres eventually fracture due to the formation of shear bands (Figure 3). It will be noted in section 2.3 that shear-dominated fibre failure can also lead to another failure mode at the ply level, entirely different from fibre kinking.

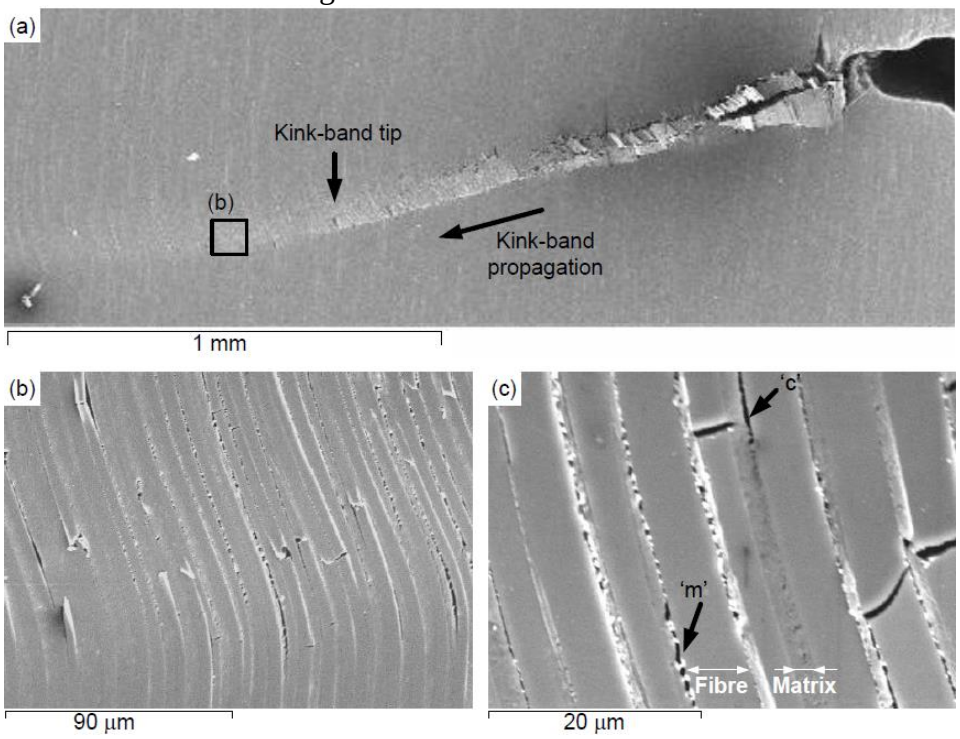

Figure 2: (a) Kink band propagating from right to left; (b) damage and localisation are visible ahead of the fully formed kink band; (c) damage in the matrix and interface [8].

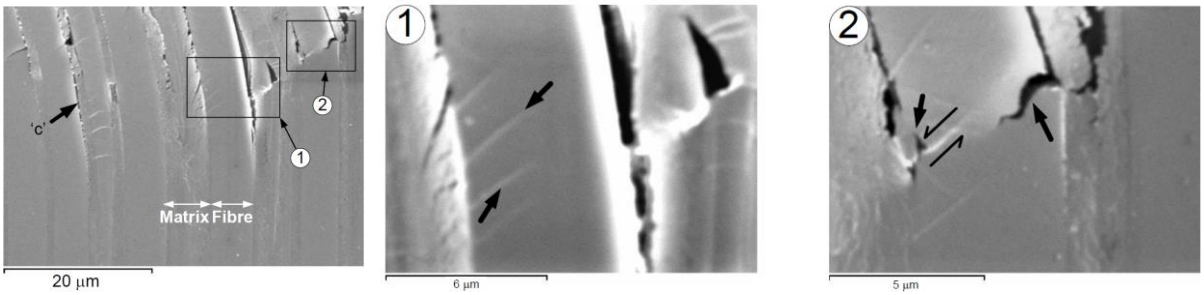

Figure 3: Failure mode of carbon fibres during kinking: shear bands form on the side of highest compressive stress at an angle ~45° with the longitudinal fibre direction [8].

2.1.2. Micromechanical FE modelling

In order to complement the qualitative experimental data detailed in section 2.1.1 and gather quantitative insight on local stress and displacement fields, kink-band formation and propagation was simulated using 2D micromechanical FE models [6]. Several modelling approaches have been used: the initial geometry of the fibres was either sinusoidal or perfectly straight (Figure 4), and different constitutive laws were investigated – cohesive or plastic formulations for the matrix, and elastic or failing fibre response.

The load versus displacement curves and the stress fields obtained (Figure 5) can be correlated with the sequence of events during kink-band formation: matrix failure occurs immediately prior to the peak load, and fibre failure only takes place much later (on the side of highest compressive stress), after most of the load-bearing capability has been lost. These results are supported by the experimental evidence in Figure 3; in addition, the fibre displacement fields obtained numerically compare well with those observed in specimens (Figure 6).

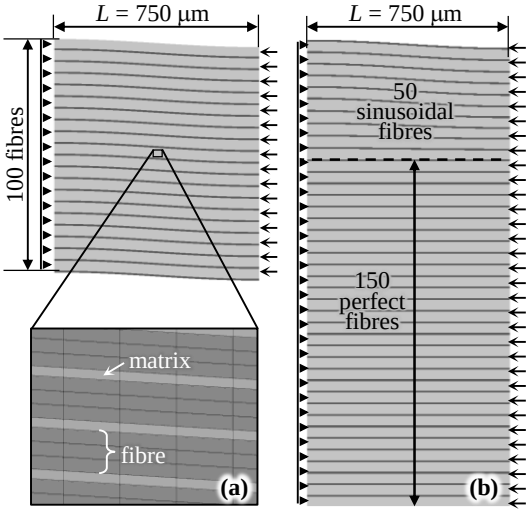

Figure 4: Micromechanical FE models for the simulation of kink bands, highlighting the initial shape of every 10th fibre: (a) baseline model with mesh detail; (b) model for kink-band propagation into initially defect-free fibres [6].

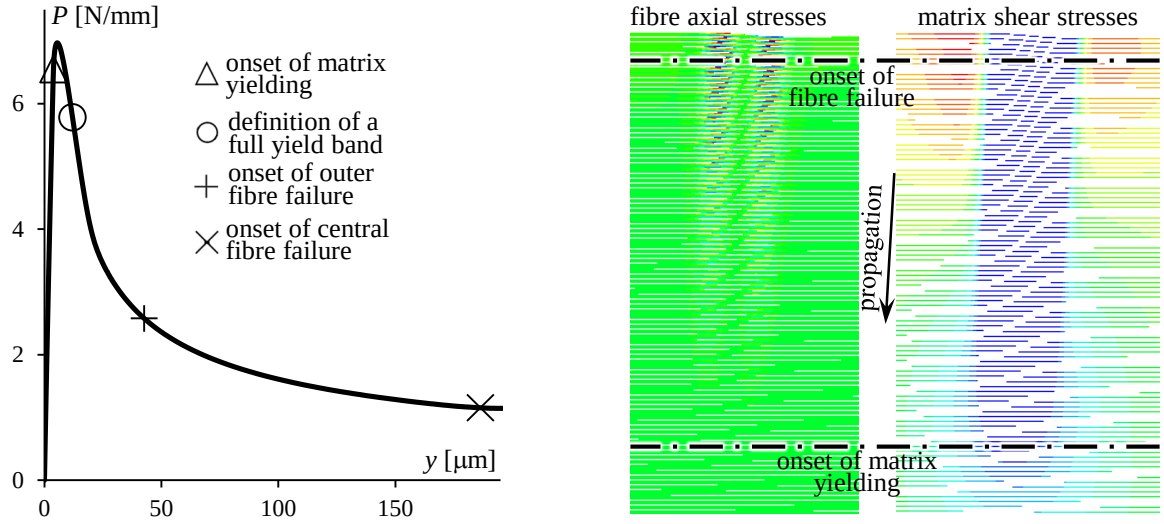

(a) Load *P* vs. fibre deflection *y* (baseline FE model).

(b) Stress fields in defect-free fibres during kink-band propagation.

Figure 5: The sequence of events for fibre kinking from the FE micromechanical models [6].

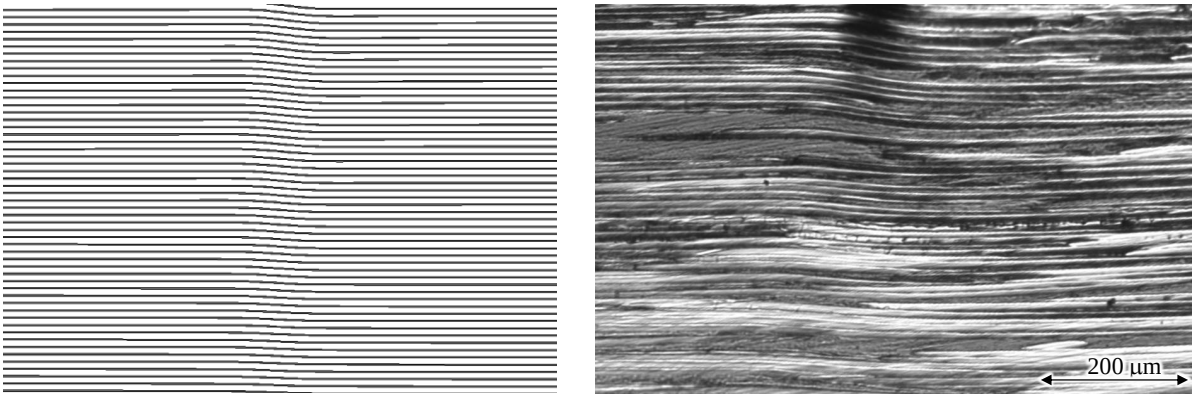

(a) Fibre deflection predicted with the FE model with initially-straight fibres

(b) Fibre deflection observed experimentally during kink-band propagation (specimen under load).

Figure 6: Fibre deflection during kink-band propagation: comparison between FE micromechanical models and experimental results [6].

2.1.3. Analytical modelling

An analytical model has been developed [9] to represent the mechanisms of kink-band formation under pure longitudinal compression, as observed experimentally (section 2.1.1) and numerically (section 2.1.2).

The model is based on the equilibrium of a fibre with a sinusoidal imperfection (y_0) along the length L. Under longitudinal compression (load P), the fibre bends (deflection y and deformed shape y_T), while being supported in shear (stresses τ) by an elasto-plastic matrix (Figure 7a). Before the onset of matrix yielding, adjacent fibres are assumed to deform in-phase; therefore, at each point x along the imperfection length, elastic shear strains in the matrix layers are related to the deformation of the fibre (deflection y, rotation θ and longitudinal displacement u in Figure 7b). The onset of matrix yielding defines the peak load and the transition to a softening domain, during which a central band of perfectly-plastic matrix grows as compression proceeds; the kink band is considered to be fully formed when fibre stresses σ_f locally reach the fibre compressive strength X_C^f.

The analytical model predicts the load versus displacement curve and the deflection and stress fields accurately; the main events for kink-band formation are predicted by the model, and a good quantitative correlation with FE results is also achieved (Figure 8). Moreover, the analytical model leads to a closed-form prediction of strength as a function of initial misalignments, and to the computation of the kink-band width at the onset of fibre failure [9].

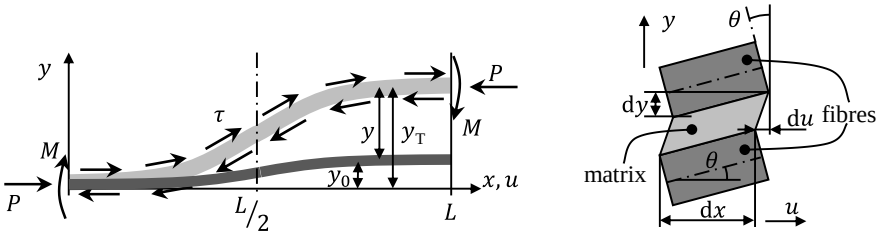

(a) Equilibrium diagram for the fibre on an elasto-plastic matrix.

(b) Definition of matrix shear strains in the elastic domain.

Figure 7: Development of the analytical model for kink-band formation under pure longitudinal compression [9].

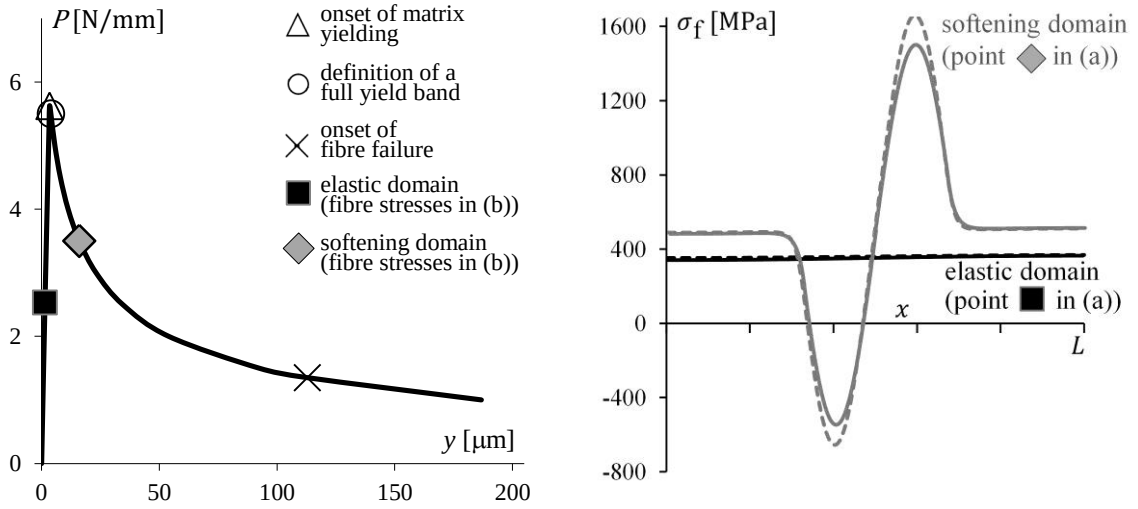

(a) Load *P* vs. fibre deflection *y* from the analytical model. Highlighted points correspond to the load for the stress fields in (b).

(b) Maximum fibre stresses σ_f along the fibre: analytical (full lines) vs. FE (dashed lines) results.

Figure 8: Results from the analytical model for kink-band formation under pure longitudinal compression [9].

2.2. Combined compression and shear

2.2.1. Experimental observations

Experimental failure envelopes for longitudinal compression and in-plane shear are not always easy to interpret due to significant scatter (Figure 9). However, it is apparent that different envelopes follow different types of trend: while the envelopes in Figure 9a and b appear to be divided in two regions with two different slopes, the envelope shown in Figure 9c appears to be characterised by only one (perhaps straight) segment while in Figure 9d the scatter is too large to extract a reasonable trend. Figure 9 therefore raises two questions: why do similar materials follow different types of trend, and could the two apparent segments observed in certain envelopes correspond to two different failure modes.

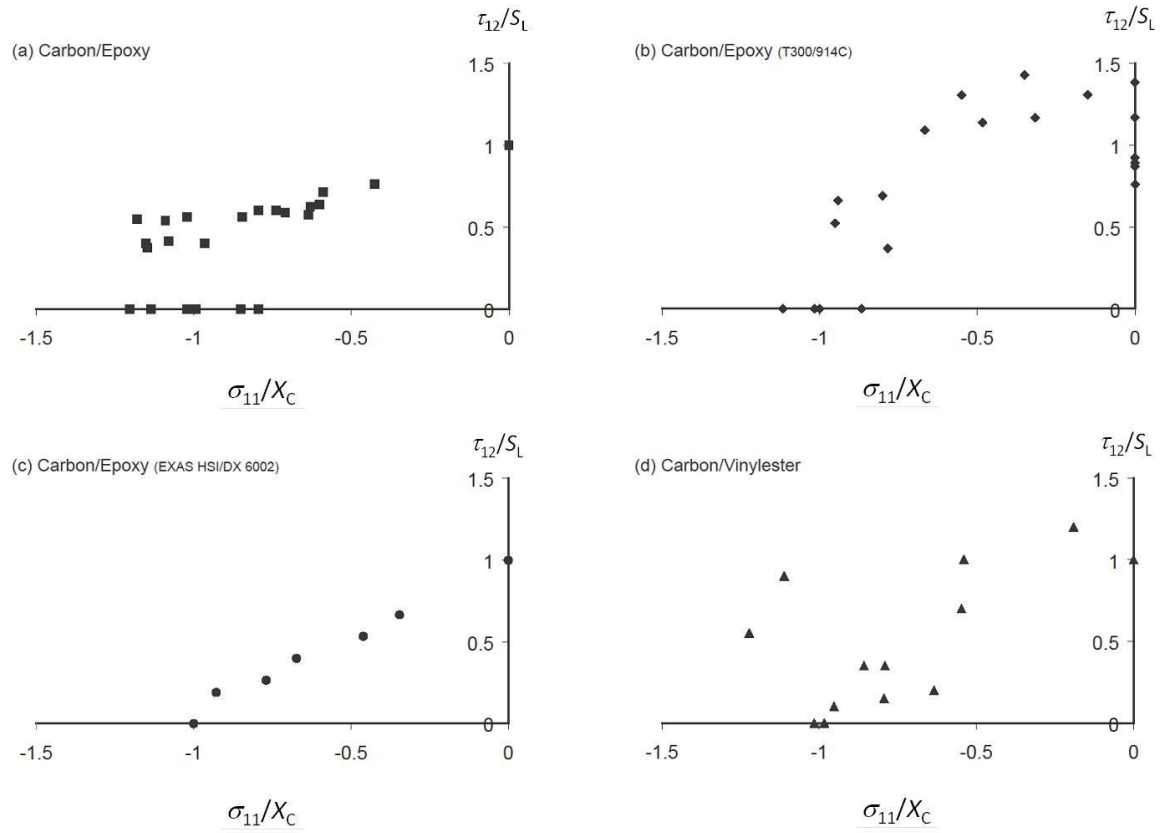

Figure 9: Comparison of failure envelopes for longitudinal compression with in-plane shear, measured by four different research groups, showing high scatter and different trends [7]. Original data from [10-13].

2.2.2. Micromechanical FE modelling

To gain insight on the mechanisms involved in the failure envelopes shown in Figure 9, micromechanical FE models have been developed. The FE model, shown in Figure 10, shares similarities to those from section 2.1.2, but because of the large number of simulations required to generate the failure envelopes, a unit cell of a matrix layer between two half-fibres is preferred. Periodic boundary conditions have been applied to the model to represent actual conditions in the composite; the nodes on each top and bottom external boundary of the half fibres are constrained so that their displacements in the x and y directions (u, v) follow

$$\forall x \in [0, L]: \begin{cases} u(x, y = d) = u(x, y = 0) \\ v(x, y = d) = v(x, y = 0) - V \end{cases} \quad \textbf{(1. 1)}$$

where V accounts for Poisson's expansion in the y-direction, and d is the dimension of the unit cell in the y direction. The model is then subjected to several combinations of longitudinal compression and in-plane shear [7]. The softening induced by matrix microcracking is represented using an elastic-plastic constitutive law for the matrix layer (with a yield strength τ_Y) and the fibres use a continuum damage model where the stress carried by the fibres in compression is reduced following a linear softening law once its strength is reached. The effect of imperfections such as initial fibre misalignment (θ_0) is also considered.

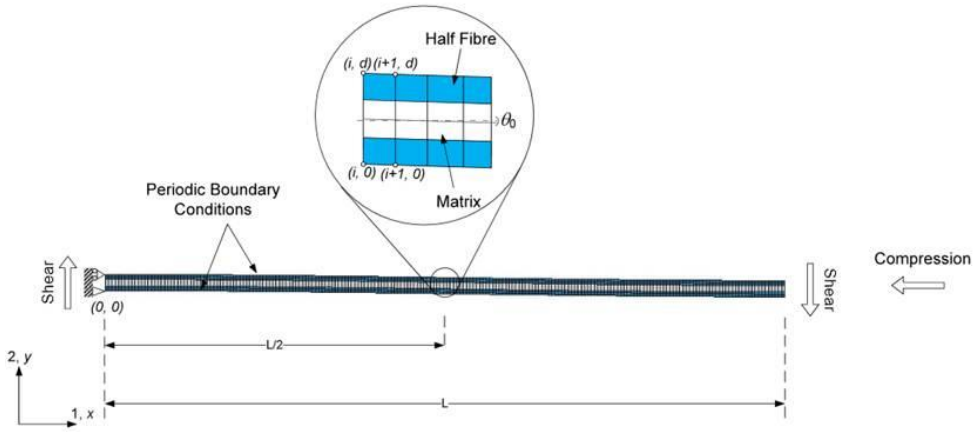

Figure 10: Micromechanical FE model with periodic boundary conditions.

The failure envelopes obtained (Figure 11) show that fibre kinking occurs in composites with large fibre initial misalignments or high fibre compressive strengths while fibre fracture can occur for materials with less significant fibre misalignments or lower fibre compressive strength X_C^f (leading in these cases to bimodal failure envelopes as in Figure 9a,b). Figure 12a and Figure 12b show that the FE model is able to reproduce accurately the different trends found experimentally [10, 11].

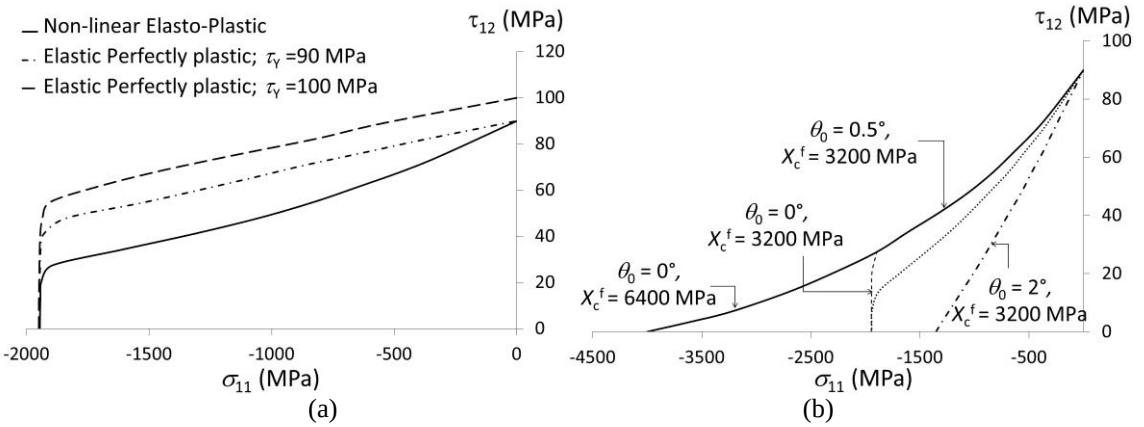

Figure 11: (a) Bimodal failure envelopes obtained using micromechanical FE models, highlighting the sensitivity to matrix constitutive properties; (b) failure envelopes highlighting the sensitivity to fibre properties [7].

For fibre kinking, the micromechanical FE models also give the width of the localised failure zone, ie. the width of the kink band (w) non-dimensionalised by the fibre diameter (ϕ_f) (Figure 12c). For the specific material properties used [7], the models predict that failure only localises into a kink band for shear stresses lower than ~75 MPa; for higher shear stresses, failure therefore corresponds to fibre/matrix splitting. Despite the significant change in localisation predicted by the FE models, the transition from fibre kinking to fibre/matrix splitting is not apparent in the numerical failure envelopes; as for example in the envelopes of Figure 11 which correspond to the predictions of Figure 12c. This also reflects the experimental findings in [10], shown in Figure 12a, where the transition from fibre kinking to fibre/matrix splitting was reported for shear stresses > 50 MPa without any change in the trend of the failure envelope.

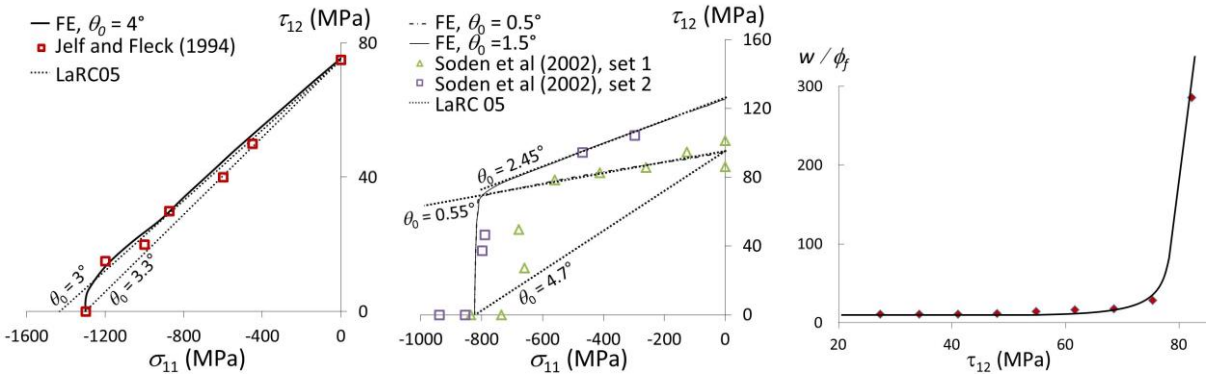

(a) (b) (c)

Figure 12: (a) and (b): Numerical predictions for bimodal failure envelopes, against experimental data [10, 11]; (c) width of a kink band during longitudinal compression with in-plane shear, as a function of applied shear stress [7].

For materials which exhibit a bimodal failure envelope for longitudinal compression combined with in-plane shear, failure under pure longitudinal compression ($\tau_{12} = 0$) is predicted as fibre compressive failure, independent from fibre kinking. Figure 3, it is also observed that failure of carbon fibres (within a kink band) results from the formation of shear bands within the fibre at angles ~45° to the fibre axis, and it was therefore inferred in section 2.1.1 that fibre fracture was a shear-dominated process. The numerical predictions and experimental observations of fibre compressive failure appear to have the same origins, and section 2.3 will discuss further how this relates to macroscopic shear failure in longitudinal compression.

2.2.3. Analytical modelling

Several theories can be used for failure predictions under combined longitudinal compression and in-plane shear; some results from these theories are shown in Figure 1c. In this section, an analytical model capable of generating such envelopes is presented [14]. The experimental observations show that kink-band initiation results from the formation of matrix microcracks and splits in the inter-fibre region (Figure 2). Therefore, the formulation of the present model is based on the hypothesis that the strength of the composite associated with fibre kinking is reached when the strain energy released per unit area of crack generated between an undamaged state and a damaged state is equal to the energy required to create the cracks (fracture energy).

To calculate the energy balance, a 2D model with unit thickness is used. The 2D model consists of a representative element of the kink band, *i.e.* a fibre of length *w* (kink-band width) embedded in a matrix (Figure 13a), onto which compressive (*P*) and shear (*S*) loads are applied. The bending contribution of the fibres is neglected and the resin is assumed to only carry shear stresses (τ). The model can also account for fibre misalignment through the introduction of the variable θ_0 as well for a nonlinear response in shear. Further details on the derivations can be found in [14].

The model leads to an interaction between longitudinal and shear loading as shown in Figure 13b and Figure 14. Figure 13b shows that the analytical predictions compare well against the results from the micromecanical FE model presented in section 2.2.2 and Figure 14 shows a good agreement of the analytical model against experimental results from the literature [10, 11]. In Figure 14b, the different levels of initial fibre misalignment corresponding to different datasets are suggested as the reason underlying the apparent scatter observed experimentally.

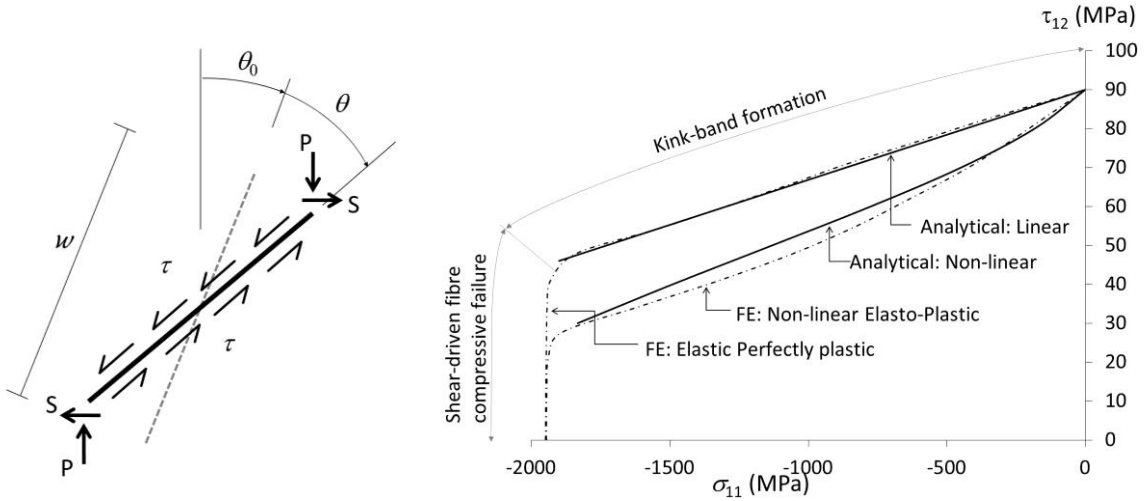

Figure 13: (a) Equilibrium of a fibre under a longitudinal compressive force and a shear force at each end, as well as a distributed shear force across the length; (b) comparison between analytical (section 2.2.3) and numerical (section 2.2.2) failure envelopes for linear and nonlinear shear responses [14].

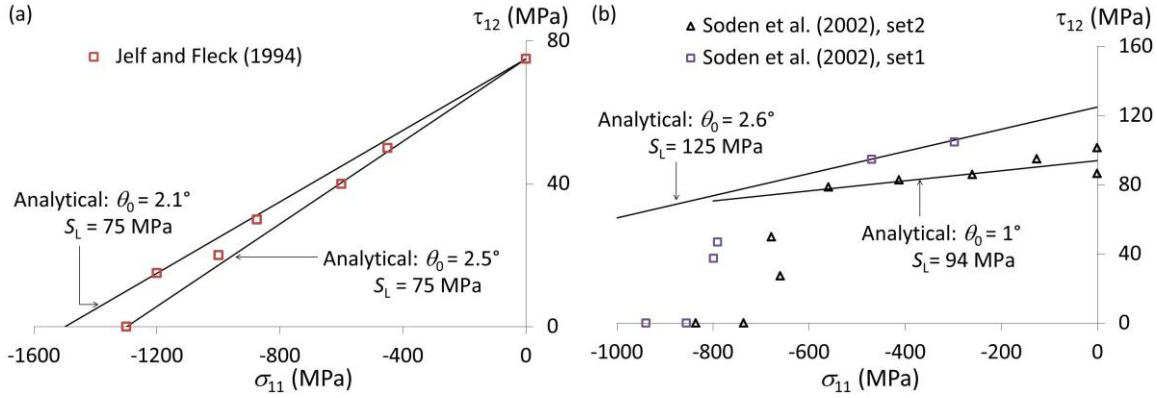

Figure 14: Failure envelopes predicted by the analytical model (section 2.2.3) [14] against experimental data [10, 11].

2.3. Another failure mode for longitudinal compression: shear-driven fibre compressive failure

2.3.1. Experimental observations

Another failure mode—brittle shear fracture at 45° to the fibres (Figure 15)—was observed experimentally [8], through developments which allowed for a greater control over the loading process during initiation. For different layups and loading rigs, the 45° fracture plane is seen to form, propagate and only then degenerate into a kink band. The transition between shear-driven fibre compressive failure and fibre kinking is particularly sharp (Figure 15).

It is hypothesised that this type of failure may be more common than expected, given that its occurrence is easily masked or lost due to the catastrophic and crushing nature of compressive failure. The different failure modes leave different features on the cross section of the broken fibres (Figure 15e, f). For instance, fibre ends at the kink-band edges show a typical bending failure pattern, with tensile (label "T" in Figure 15e) and compressive (label "C" in Figure 15e) failures separated by a neutral axis, while for shear-driven fibre compressive failure, the fibre ends are smooth and show significant abrasion (Figure 15f).

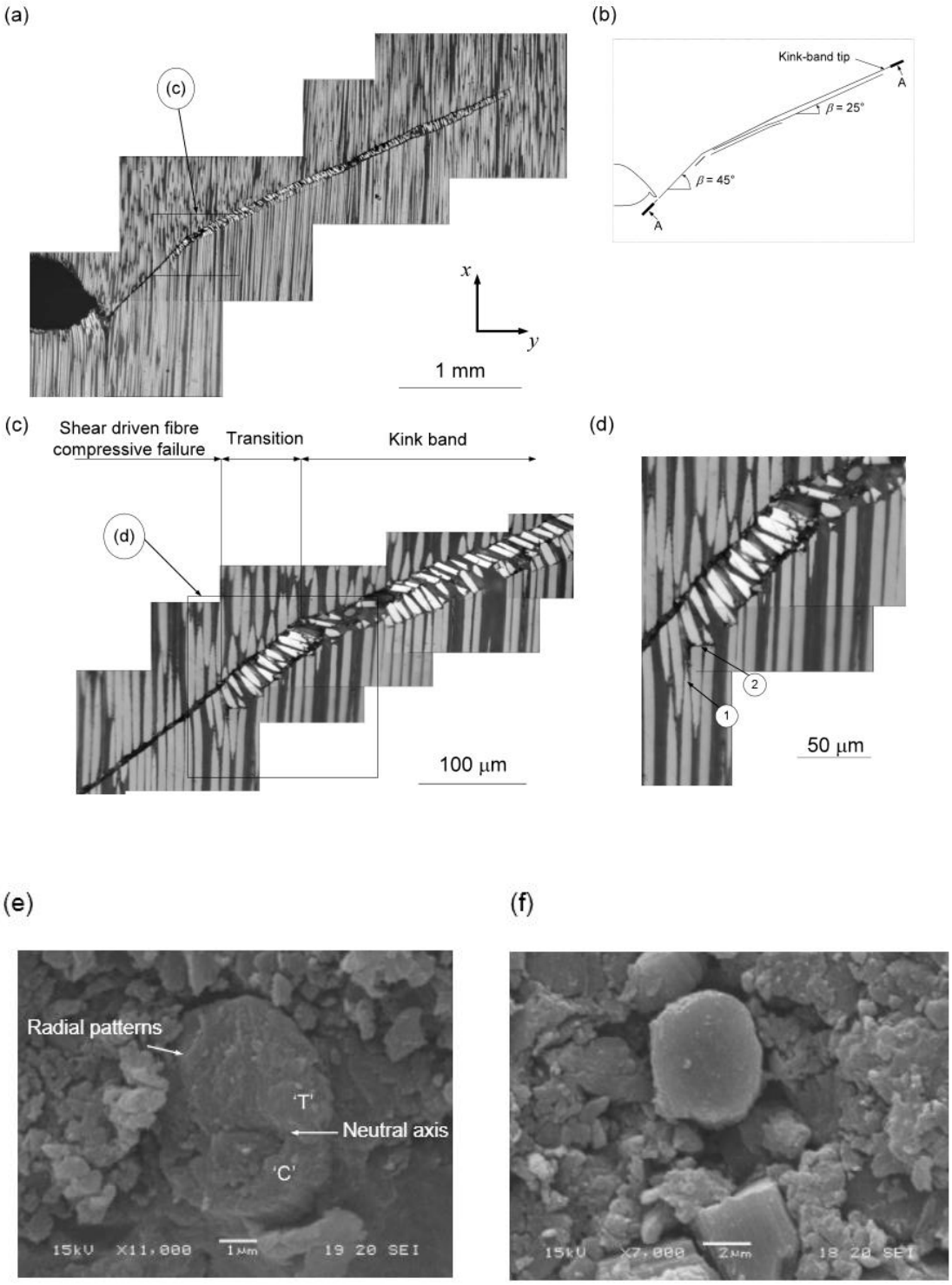

Figure 15: (a)-(d) Shear-driven fibre compressive failure as an independent failure mode which eventually leads to kink-band formation; (e) bending failure of a fibre during kink-band formation and (f) broken fibre in the shear-driven fibre compressive failure region [8].

2.3.1. Modelling

The modelling of shear-driven fibre compressive failure can be easily achieved using in a first instance a maximum shear criterion, resulting in combined envelopes for shear-driven fibre compressive failure / fibre kinking / splitting as shown in Figure 16.

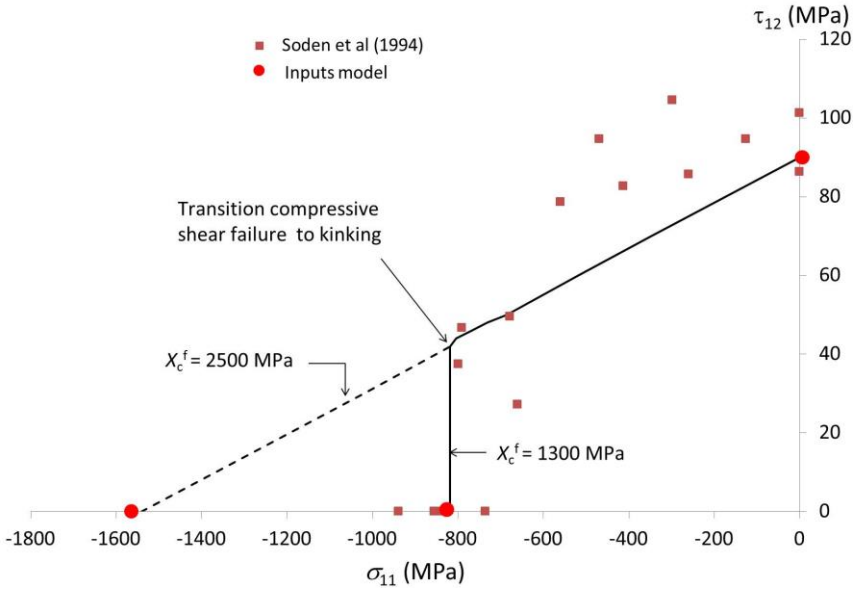

Figure 16: Complete failure envelope prediction for combined longitudinal compression and in-plane shear [14].

3. Compressive failure in woven composites

3.1. Experimental observations

Experimental studies analogous to those on UD were carried out for woven composites [15]. Different reinforcement architectures were tested under compression: 2×2 twill and 5H satin. Kinking was identified as the mechanism responsible for the failure of the load-aligned tows (Figure 17a). The latter have a structural role within the reinforcement architecture, highlighted in Figure 17b where tows are observed to fail individually. Moreover, the reinforcement architecture was seen to affect the failure morphology and immediate sequence of events [15]. One of the observed differences in failure morphology is highlighted in Figure 18; while 2×2 twill tows tended to fail at the centre of the crimp region ($d \approx 0$), 5H satin tows failed systematically at a distance $d \neq 0$ from it.

In a 2D woven laminate, shifting between adjacent layers is usually not controlled, leading to a random configuration (Figure 19a). Upon compression, adjacent layers will naturally interact. This interaction, namely the out-of-plane support provided by the adjacent layers, was also investigated. Several specimens were produced with carefully aligned adjacent layers in an In-Phase (IP) configuration, i.e. all load-aligned tows of adjacent layers are In-Phase (Figure 19b). Figure 20 shows that the failure morphology changes significantly with the support provided by the adjacent layers. As highlighted previously, tows behave as structural elements within the reinforcement architecture; under compression, the out-of-plane support provided by the adjacent layers affects the bending of the tows and consequently the failure morphology. This effect was also seen to be a function of the reinforcement architecture [15].

At the microscale, compressive failure of woven composites occurs according to the process previously described for UD: microcracking/plasticity of the matrix between fibres (within the tows or at the interface between tows and pure matrix regions) leading to kinking/splitting (Figure 21).

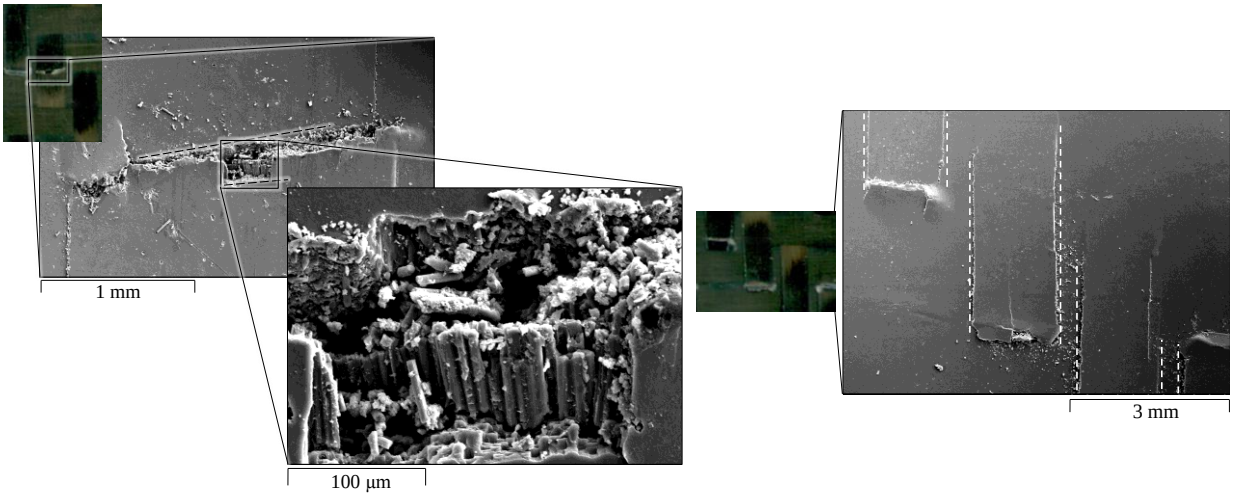

(a) **(b)**

Figure 17: (a) Tow failed by kinking, (b) several tows failing individually [15].

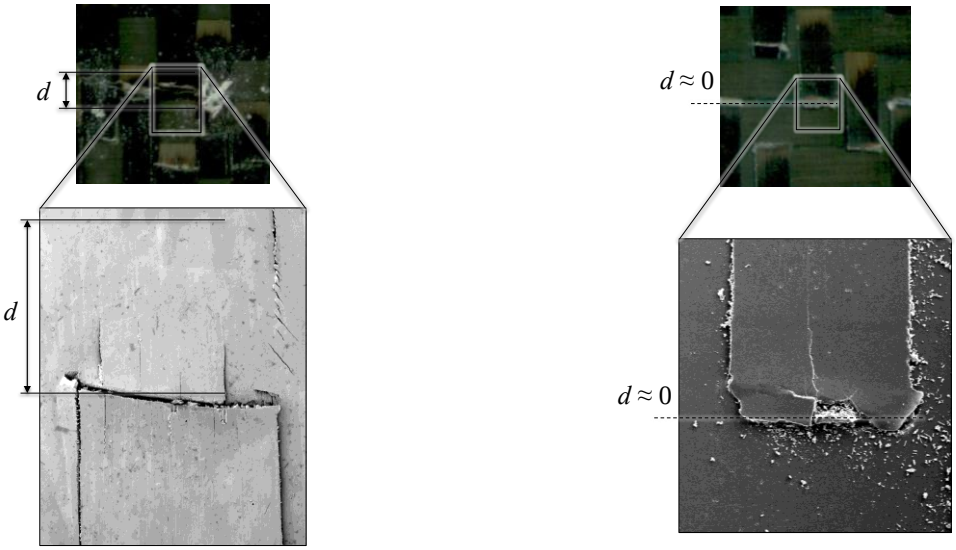

(a) 5H satin: tows failed at a distance $d \neq 0$ from the centre of the crimp region. **(b) 2×2 twill: tows failed at a distance $d \approx 0$ from the centre of the crimp region.**

Figure 18: Differences in failure location between different reinforcement architectures: 2×2 Twill and 5H Satin [15].

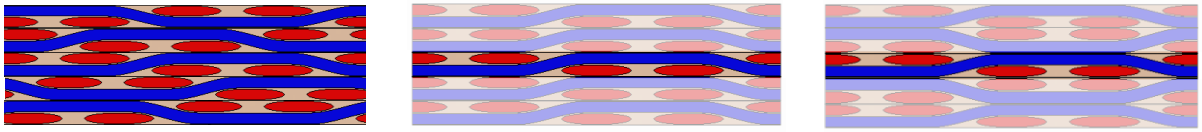

(a) Random-stacked **(b) In-phase (IP)** **(c) Out-of-phase (OP)**

Figure 19: Cross-sections of random-stacked, In-Phase and Out-of-Phase laminates.

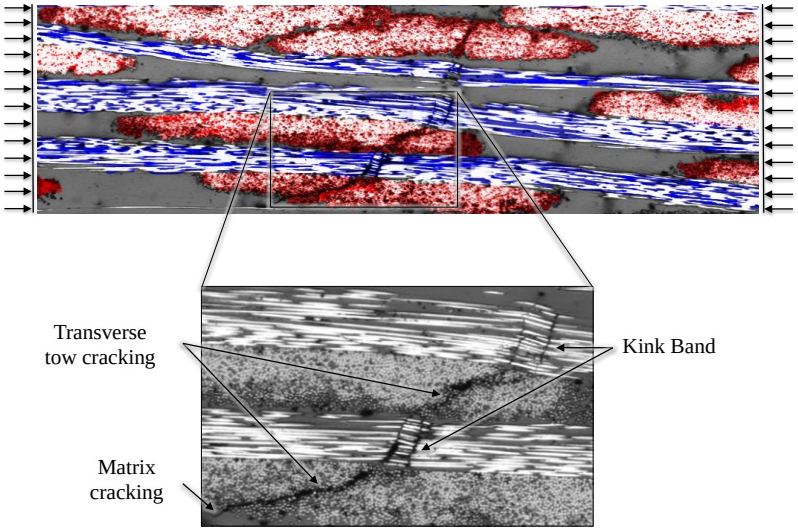

(a)

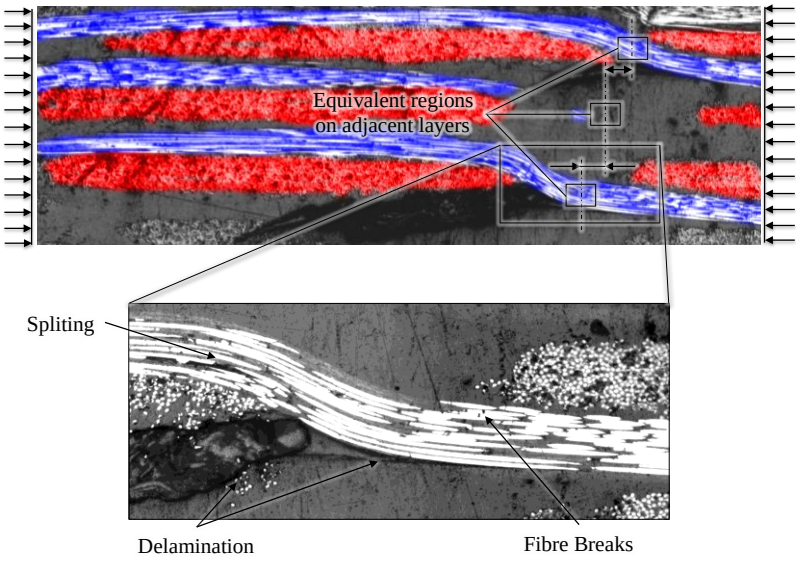

(b)

Figure 20: Longitudinal compression in a 2x2 twill composite [15]. (a) Random stacking and (b) In-phase stacking.

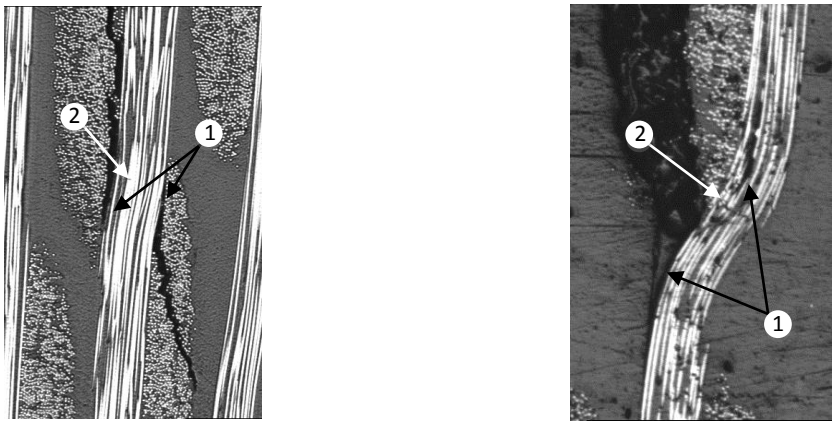

(a) 5H Satin **(b) 2×2 Twill**

Figure 21: At the microscale, compressive damage starts with microcracking/plasticity of the matrix leading to splitting (1) at the interface of the load-aligned tows and/or within the tows. The first fibre failures (2) occur soon after. Further loading leads to the development of kink bands.

3.2. Numerical and analytical modelling

A finite element model of a 2×2 twill reduced Unit Cell (rUC) was developed [16] (Figure 22a). The rUC used is the smallest possible domain that can be used to analyse a 2×2 twill geometry, whilst applying the correct periodic boundary conditions both in-plane and out-of-plane [17]. In the out-of-plane direction, two sets representing different cases of out-of-plane support were applied: i) In-Phase (IP), where all load-aligned tows of adjacent layers are IP, and ii) Out-of-Phase (OP), where all load-aligned tows of adjacent layers are OP (Figure 19b and c), respectively. These two cases define practical limits of support that any layer can have within a laminate, where adjacent layers are randomly shifted. The tows are modelled as an orthotropic material, with the material orientations following the central path of the tow. The matrix is considered to be an elasto-plastic material and its response is modelled using a linear Drucker-Prager plasticity model. Additionally, the debonding between tows and matrix is accounted for and modelled through the definition of cohesive contact. The longitudinal compressive failure is predicted using a kinking model [18], developed for UD materials, applied at the tow level. The use of such model to predict the compressive failure of woven composites is in agreement with what is found experimentally, where compressive failure is seen to occur by kinking of the load-aligned tows (e.g. Figure 17). The material is assumed to fail when failure of the load-aligned tows is detected using the referred criterion.

With the insight gathered from both experimental and numerical investigations, an analytical model was also developed [19,20] (Figure 22b). It consists of an Euler-Bernoulli beam supported by an elastic foundation. The beam represents the load-aligned tow and is regarded as an UD composite. The elastic foundation provides both normal and torsional support, and its properties are derived from kinematic models that account for: weave effect, case of support provided by the adjacent layers (IP or OP) and elastic properties of the tows and matrix, Figure 23.

The weave effect (Figure 23a) is accounted for by considering that the in-plane adjacent tows affect the deflection of each other through the shearing of the matrix connecting them. The latter is obtained realizing that the deflection of adjacent tows can be related, having into account that equivalent positions in adjacent tows displace in the same fashion [17]. Having determined the shearing of the connecting matrix, the distributed load exerted in a given tow by the adjacent tows can be approximated by:

$$p_{weave}(x) = 2\frac{(y_0 + \bar{t}_{tow})}{g} G_m v(x) \quad \textbf{(2. 1)}$$

where y_0 is a geometrical parameter (Figure 22b), $\bar{t}_{tow}$ represents the average tow thickness over the cross-section of the tow, g is the gap between adjacent tows, G_m is the shear modulus of the matrix and $v(x)$ is the deflection of the tow.

The kinematic model that accounts for the IP support is illustrated in Figure 23b. In this case, the support is essentially provided by the shearing of the material (matrix and transverse tows) between load-aligned tows. Assuming that all load-aligned tows from adjacent layers displace in an identical fashion (Figure 23b), the shear strain of the material between tows can be obtained from geometrical considerations, as a function of the tow deflection. Knowing the shear strain, the shear stress applied to a given tow can be determined by:

$$\tau_{IP}(x) = G_h \left(1 + \frac{\bar{t}_{tow}}{h}\right) \frac{dv}{dx} \quad \textbf{(2. 2)}$$

where G_h is the modulus of the material between tows, homogenised using the rule of mixtures, and h is the average thickness of the material between tows. Additionally, the gradient of equation (2. 2) leads to a direct pressure applied to the tow given by:

$$p_{d\tau/_{dx}}(x) = -\frac{d\tau}{dx} h \cdot b_{tow} \quad \textbf{(2. 3)}$$

where b_{tow} is the width of the tow. This gradient is obtained from the equilibrium of the material between tows [20].

In the OP configuration (Figure 23c), the support is mainly provided by the straining of the material between load-aligned tows, due to their deflection in opposite directions. Similarly to the IP case, the strain of the region between tows can be obtained from geometrical considerations (Figure 23c). Knowing the strain, the pressure p_{adj}, applied by the load-aligned tows of the adjacent layers, is obtained by:

$$p_{adj} = 2v(x)b_{tow}\left(\frac{E_h^{Top}\left(1-\nu_h^{Top}\right)}{\left(1-\nu_h^{Top}\right)\left(1-2\nu_h^{Top}\right)h^{Top}} + \frac{E_h^{Bot}(1-\nu_h^{Bot})}{(1-\nu_h^{Bot})(1-2\nu_h^{Bot})h^{Bot}}\right) \quad \textbf{(2. 4)}$$

where $E_h^{Top/Bot}$ and $\nu_h^{Top/Bot}$ are the homogenized Young moduli and Poisson ratios, and $h^{Top/Bot}$ is the distance between the adjacent tows. The superscripts *Top* and *Bot* refer to the regions above and below a given tow, respectively. Finally, the governing differential equation is derived in a general fashion from the analysis of the equilibrium of a beam element (Figure 24):

$$\frac{d^4v(x)}{dx^4} + \lambda_{1-IP/OP}^2 \frac{d^2v(x)}{dx^2} + \lambda_{2-IP/OP}^2 v(x) = -\lambda_3^2 \frac{d^2y_0(x)}{dx^2} \quad \textbf{(2. 5)}$$

where $\lambda_{i-IP/OP}$ are a function of the case of support (IP/OP) considered, and $y_0(x)$ is the initial shape of the tow.

Figure 25a compares the numerical and analytical results for the shear along the tow centre line obtained for the IP case. The good agreement indicates that the analytical model developed captures well all the key of the weave response under compression. Figure 25b compares the numerical and analytical compressive strength predictions with the experiments. The numerical and analytical predictions are obtained by averaging the strength predictions for the IP and OP cases. The analytical and numerical models show accurate strength predictions (within the scatter of the experiments). Nevertheless, the numeric model shows better agreement with experiments. This is attributed to the more accurate stress fields obtained numerically and to the modelling of the non-linear response of the matrix. It is worth highlighting that the non-linear material response can be included in the analytical model. However, the governing differential equation would have to be solved iteratively/numerically, thus compromising the simplicity of the proposed model. The analytical model has runtime of less than two seconds in its current form. This is extremely beneficial when performing parametric/stochastic studies.

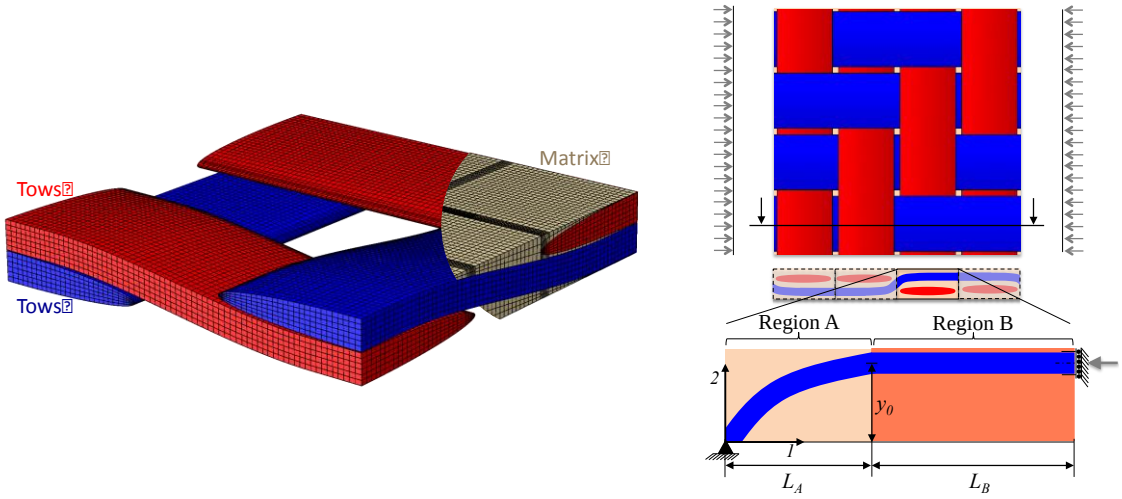

(a) **(b)**

Figure 22: (a) Finite element model of a 2×2 Twill reduced Unit Cell, (b) Analytical model; the geometry of the tow is approximated by a sinusoidal beam connected with a straight beam, Regions A and B respectively [16, 19, 20].

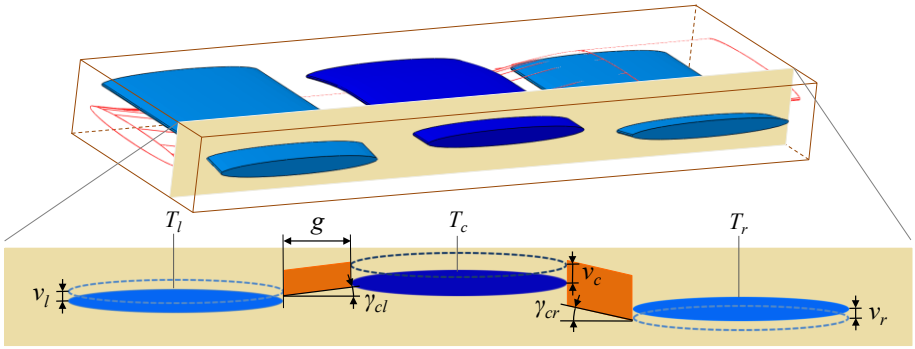

(a) weave effect: shearing of the matrix connecting in-plane adjacent tows, (of the same woven layer). v_l, v_c and v_r represent the deflection of the tows T_l T_c and T_r, respectively; γ_{cl} and γ_{cr} are the shear strain of the matrix connecting T_c to T_l and T_r.

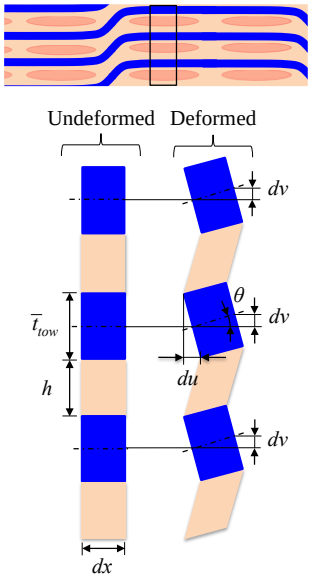

(b) In-phase: shearing of the material between load-aligned tows of adjacent layers.

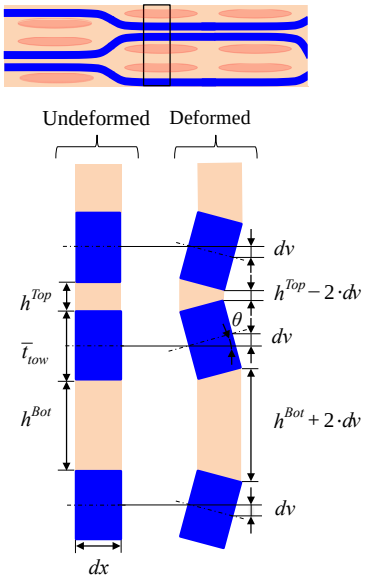

(c) Out-of-phase: straining (through-thickness direction) of the material between tows of adjacent layers

Figure 23: Kinematic models used to derive the properties of the elastic foundation [19, 20].

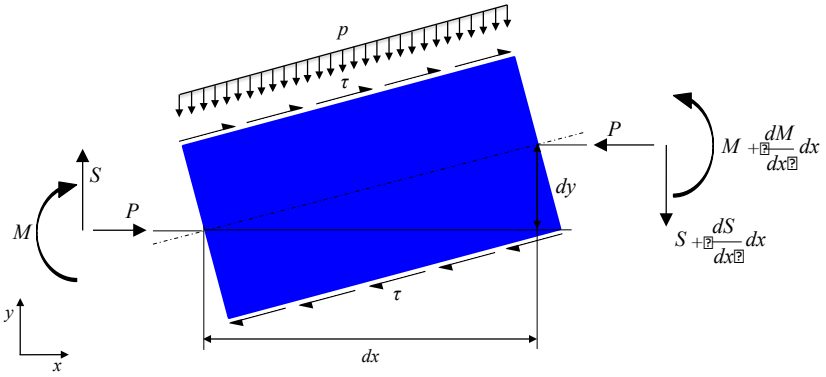

Figure 24: Equilibrium of a beam element. *P* is the load applied; *M* and *S* represent the moment and shear force; *p* and *τ* denote the pressure and shear applied to the tow by the elastic foundation [19, 20].

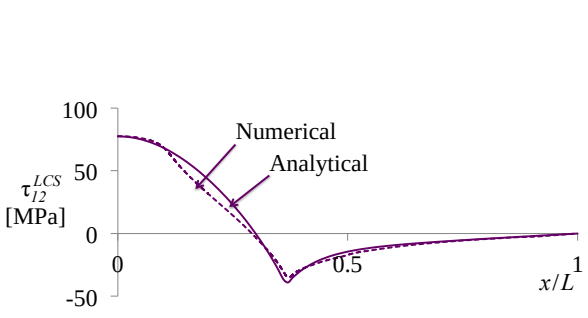

(a) Analytical and numerical predictions for the shear along the centre of the tow (In-Phase) given in the Local Coordinate System (LCS) aligned with the centre line of the tow; homogenized strain applied $\varepsilon_1 = -0.008$.

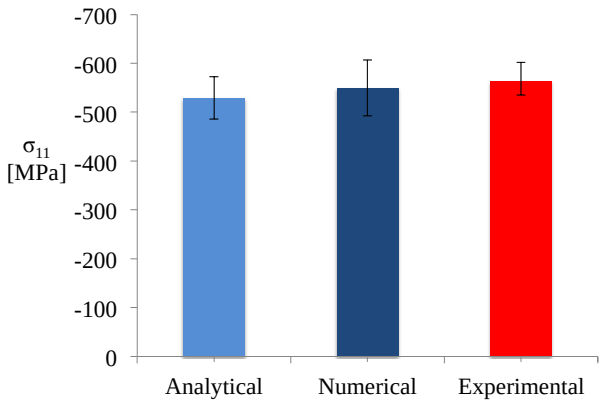

(b) Comparison between the analytical, numerical and experimental results for the compressive strength. In the analytical and numerical predictions, the limits of the error bars min/max correspond to the results obtained with IP/OP cases, respectively.

Figure 25: Comparison between numerical, analytical and experimental results [16, 19, 20].

4. Compressive failure in recycled composites

4.1. Introduction

In recent decades, the exponential increase in the use of CFRP has motivated the development of recycling technologies for the ever increasing amount of CFRP waste produced. It is suggested that recycling CFRP can bring environmental and economic benefits over the traditional methods of landfilling and incineration. Recent studies [21] have also shown that recycled (r-) CFRP can replace traditional materials with weight savings in selected structural applications, such as non safety-critical components in the aeronautical and automotive industries currently manufactured with aluminium or glass-fibre.

Recycled composites are manufactured by re-impregnating recycled carbon fibres with a new resin. The recycling step typically consists of a thermal or chemical process to break down the matrix and release the valuable carbon fibres, either from end-of-life components or manufacturing waste.

Due to the reprocessing, recycled composites present distinct features from those of their virgin precursors, namely regarding the micromechanical properties of constituents (fibres and interface) and the reinforcement architecture. Such specificities require then the development of dedicated material models and design methods for rCFRPs. However, despite their significant differences, the mechanisms involved in the compressive failure of recycled composites share many features with UD and woven composites (detailed in sections 2 and 3). This section discusses similarities and differences between the compressive failure of two types of recycled CFRP and their virgin counterparts.

4.2. Short-fibre recycled composites

Most rCFRPs have a short-fibre randomly oriented architecture. However, contrarily to most of virgin short-fibre composites, the recyclates typically present a multiscale reinforcement architecture, with individually dispersed fibres and fibre bundles; these bundles are held together by residual matrix not removed during the recycling (Figure 26).
Compressive failure of recycled composites with such architecture is complex [19]. In areas with no bundles (Figure 27a, b), a fracture plane starts forming at low angles (β<20°) and then rotates up to ~54° through plastic deformation of the matrix. In areas with bundles, the failure process resembles the failure of tows in woven composites: isolated bundles fail by bending (Figure 27c), while kink bands are formed whenever neighbouring bundles provide sufficient support (Figure 27d).

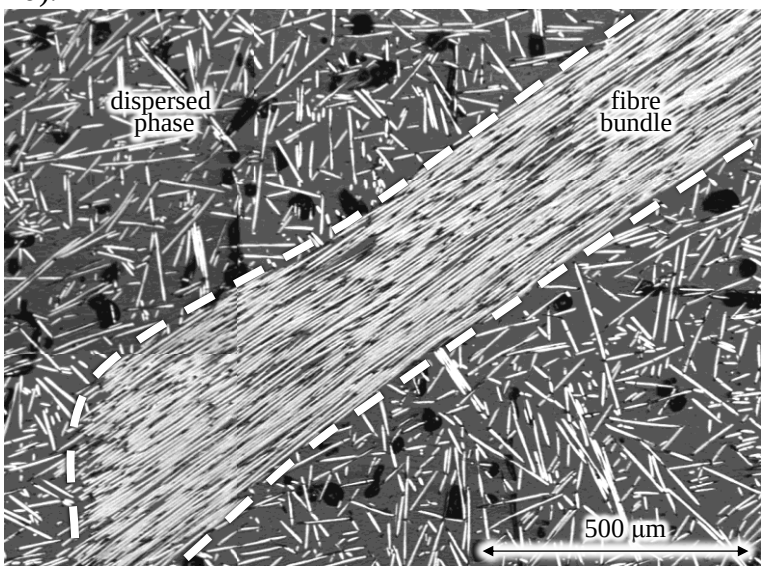

Figure 26: Recycled composite with a multiscale structure consisting of fibre bundles in a short-fibre-reinforced matrix [22].

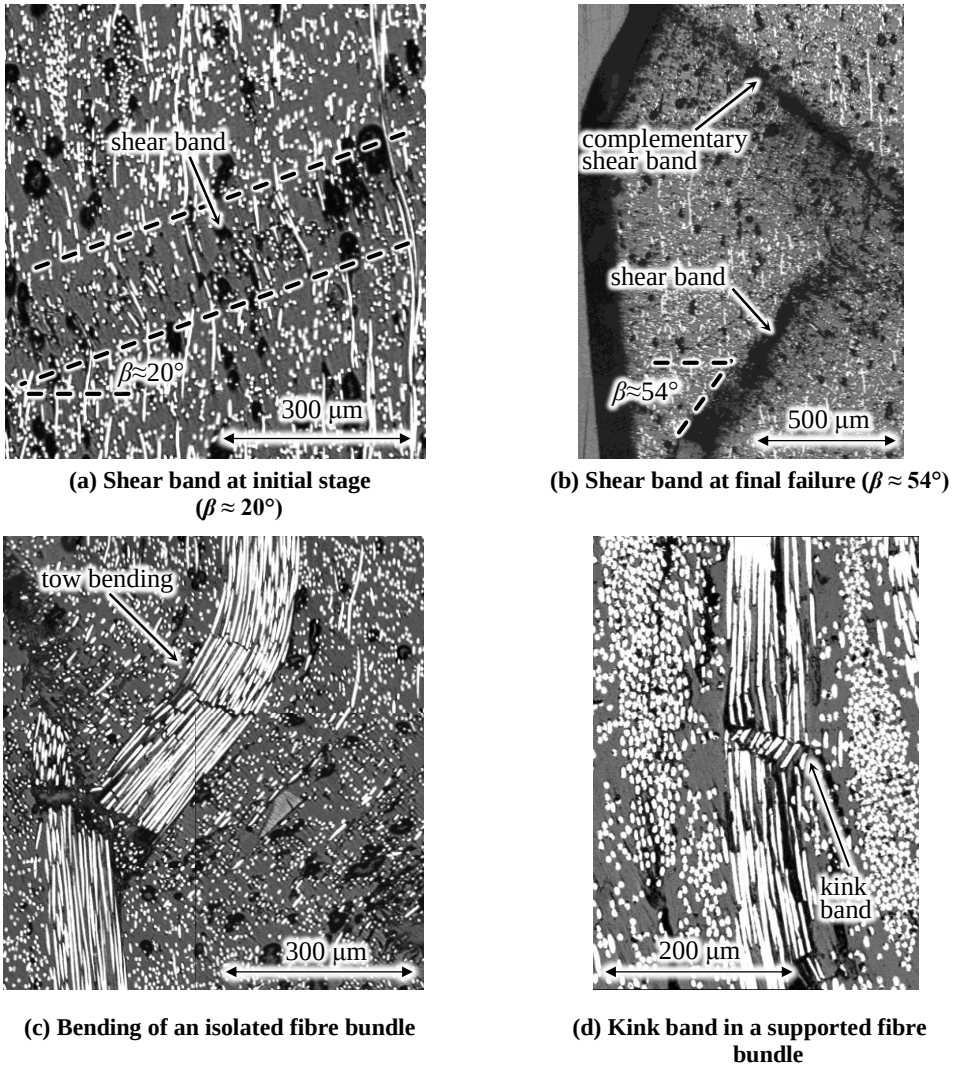

(a) Shear band at initial stage ($\beta \approx 20°$)

(b) Shear band at final failure ($\beta \approx 54°$)

(c) Bending of an isolated fibre bundle

(d) Kink band in a supported fibre bundle

Figure 27: Compressive failure of short-fibre rCFRPs with fibre bundles [22].

4.3. Woven recycled composites

To further investigate the effect of fibre recycling on the performance of rCFRPs, samples of out-of-date woven prepreg were recycled under different pyrolysis conditions, and re-impregnated into woven rCFRPs mimicking the architecture of the virgin composite (the 5 harness satin woven analysed in section 3). Both virgin and recycled materials were characterised, at the filament and composite levels [23].

In spite of the severe fibre strength degradation occurring during the most aggressive reclamation cycles, fibre stiffness remained relatively unchanged (Figure 28a); these results at the filament level were directly replicated on the tensile performance of the composite (Figure 28b). However, the compressive strengths of the rCFRP and virgin CFRP were statistically the same (Figure 28c), and the failure features are remarkably similar (Figure 28d).

The fact that the compressive strength of a woven CFRP is independent of its tensile strength – at both fibre and composite levels – suggests that fibre kinking is indeed governed by the failure of the resin or fibre-matrix interface, rather than by the tensile failure of the fibres themselves. Moreover, it was shown that rCFRPs can assume unique combinations of mechanical properties, underlining the need for specific models and design methods for these materials.

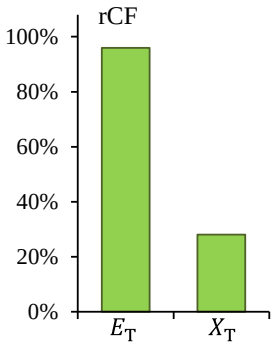

(a) Recycled fibre properties: retention of modulus (E_T) and strength (X_T) relatively to virgin fibre.

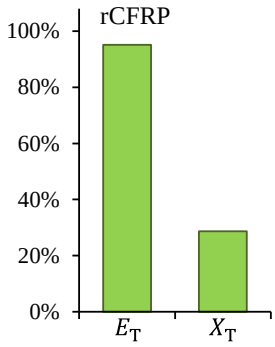

(b) Recycled CFRP tensile properties: retention of modulus (E_T) and strength (X_T) relatively to virgin composite.

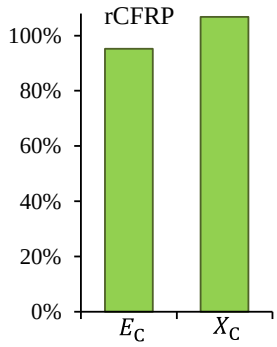

(c) Recycled CFRP compressive properties: retention of modulus (E_C) and strength (X_C) relatively to virgin composite.

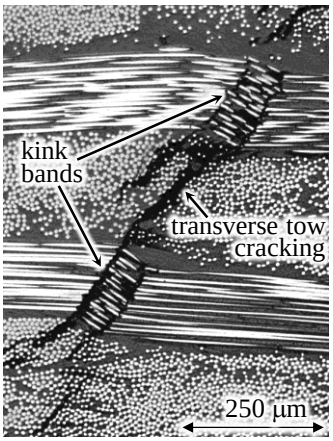

(d) Morphology of compressive failure

Figure 28: Mechanical response of a woven rCFRP: the compressive performance at the recycled-composite level is shown to be insensitive to fibre strength degradation, occurred in the most aggressive recycling conditions.

5. Overall discussion

It is found that there are two competing mechanisms for longitudinal compressive failure in UD composites: the widely documented kink-band formation (also referred to in the literature as microbuckling), and (the much less documented) shear failure of the fibres at a ~45° angle to the loading direction. Both mechanisms can be described analytically by resolving the stress field at the fibre and matrix level, with the fibres idealised as beams, leading to predictions for failure stresses and morphologies in agreement with experimental observations.

Despite their more complex architecture, woven composites under longitudinal compression exhibit similar failure morphologies to those in UD composites, thus suggesting similar mechanisms (compare Figure 2 and Figure 15 for UD to Figure 20 and Figure 21 for woven). The analytical treatment is in this case made more difficult by not only the morphology of the weave, but also by the uncertainty related to the exact stacking configuration, and hence through-the-thickness support provided to a given layer. Analytical models for extremes of this support (in-phase and out-of-phase stacking), whereby the tows are idealized as beams, are however shown to accurately capture the stress fields within the tows. In turn, combining these stress fields in the tows with models for fibre kinking originally developed for UD composites leads to compressive strength predictions in agreement with experiments and

finite element results. This confirms that the failure mechanisms for UD and woven composites under longitudinal compression are intrinsically physically similar.

Recycled composites which preserve the original woven architecture of the weave hold the potential to provide further insight into the validity of analytical models. In fact, a common denominator for fibre kinking models (those presented herein but also most in the literature) is that strength depends strongly on the strength/ toughness of the matrix and interface, but not on the strength of the fibres. By varying the thermo-chemical parameters of the recycling process, it is possible to manufacture different recycled woven composites which are essentially the same, but with varying fibre strength. Experimentally, it was found that reducing the fibre strength by ~80% has virtually no effect on the compressive strength of the composite (Figure 28a, b and c), while it has, obviously, dramatic effects in tension. Additionally, the morphology of the failure process in these woven composites with much lower tensile fibre strength (Figure 28d) is remarkably similar to that in virgin woven composites (Figure 20 and Figure 21). This finding, obtained using recycled composites, provides a strong indication for the wide range of applicability of the models currently available for fibre kinking in virgin UD and woven composites.

Recycled composites also present a wealth of novel reinforcement architectures; this offers new challenges both for understanding and modelling their compressive failure. One such type of architecture consists of a matrix reinforced by randomly dispersed short fibres and bundles of different dimensions (Figure 26), effectively providing reinforcement to the matrix over several scales. The bundles in these materials exhibit failure mechanisms similar to those in UD (compare Figure 27 to Figure 2 and Figure 15) and woven composites (compare Figure 20 and Figure 21). This suggests that analytical models for compressive failure of these novel materials ought to be based on the same principles adopted for the traditional architectures.

6. Conclusions

The first part of this paper presents experimental and micromechanical FE studies which were conducted with the aim of developing analytical models for longitudinal compressive failure in UD composites. Predictions from such models are shown to compare favourably with the numerical and experimental results. The existence and importance of a shear-driven fibre compressive failure mode under longitudinal compression is highlighted, as it is shown to be critical for explaining different trends observed in experimental failure envelopes.

Woven composites show some similarities to UD composites in their longitudinal compressive failure modes. In particular, it is shown that once the stress field is resolved in the tows, fibre kinking models originally developed for unidirectional composites can be successfully applied to woven composites. However, in obtaining the stress field in the tows, woven composites also show some added complexity such as the dependence of the failure process on the through-the-thickness support provided by the adjacent layers.

Experimental results using woven composites with very weak recycled fibres suggest that the longitudinal compressive strength of woven composites does not depend on tensile fibre strength. This finding is in agreement with the models presented, which do not depend on that variable for fibre kinking. The similarities in the longitudinal compressive failure processes of different materials, regardless of their exact microstructure, suggest that knowledge and experience gathered in recent decades in analysing advanced composites appears to be very valuable for the analysis of novel types of composites, such as recycled composites with multiscale fibre bundle reinforcement.

Acknowledgement

Different parts of this work were funded by EPSRC, DSTL, Airbus and Renault F1 (EP/E0Z3169/1), as well as FCT (SFRH/BD/36636/2007and SFRH/BD/44051/2008).

References

[1] Rosen, B. W. 1965 Mechanics of composite strengthening. In *Fiber Composite Materials*, chapter 3, pp. 37-75. Ohio: American Society of Metals.

[2] Argon, A. S. 1972 Fracture of composites. In *Treatise on Materials Science and Technology*, vol. 1, pp. 79-114. New York: Academic Press.

[3] Budiansky, B., Fleck, N. A. & Amazigo, J. C. 1998 On kink-band propagation in fiber composites. *Journal of the Mechanics and Physics of Solids* **46**(9), 1637-1653. (DOI 10.1016/S0022-5096(97)00042-2.)

[4] Fleck, N. A., Jelf, P. M. & Curtis, P. T. 1995 Compressive failure of laminated and woven composites. *Journal of composites technology & research* **17**(3), 212-220.

[5] Soutis, C., Fleck, N. A. & Smith, P. A. 1991 Failure prediction technique for compression loaded carbon fibre-epoxy laminate with open holes. *Journal of Composite Materials* **25**(11), 1476-1498.

[6] Pimenta, S., Gutkin, R., Pinho, S. T. & Robinson, P. 2009 A micromechanical model for kink-band formation: Part I - Experimental study and numerical modelling. *Composites Science and Technology* **69**(7-8), 948-955. (DOI 10.1016/j.compscitech.2009.02.010.)

[7] Gutkin, R., Pinho, S. T., Robinson, P. & Curtis, P. T. 2010 Micro-mechanical modelling of shear-driven fibre compressive failure and of fibre kinking for failure envelope generation in CFRP laminates. *Composites Science and Technology* **70**(8), 1214-1222. (DOI 10.1016/j.compscitech.2010.03.009.)

[8] Gutkin, R., Pinho, S. T., Robinson, P. & Curtis, P. T. 2010 On the transition from shear-driven fibre compressive failure to fibre kinking in notched CFRP laminates under longitudinal compression. *Composites Science and Technology* **70**(8), 1223-1231. (DOI 10.1016/j.compscitech.2010.03.010.)

[9] Pimenta, S., Gutkin, R., Pinho, S. T. & Robinson, P. 2009 A micromechanical model for kink-band formation: Part II - Analytical modelling. *Composites Science and Technology* **69**(7-8), 956-964. (DOI 10.1016/j.compscitech.2009.02.003.)

[10] Jelf, P. M. & Fleck, N. A. 1994 The failure of composite tubes due to combined compression and torsion. *Journal of Materials Science* **29**(11), 3080-3084. (DOI 10.1007/BF01117623.)

[11] Soden, P. D., Hinton, M. J. & Kaddour, A. S. 2002 Biaxial test results for strength and deformation of a range of E-glass and carbon fibre reinforced composite laminates: failure exercise benchmark data. *Composites Science and Technology* **62**(12-13), 1489-1514. (DOI 10.1016/S0266-3538(02)00093-3.)

[12] Yerramalli, C. S. & Waas, A. M. 2003 A failure criterion for fiber reinforced polymer composites under combined compression-torsion loading. *International journal of solids and structures* **40**(5), 1139-1164. (DOI 10.1016/S0020-7683(02)00649-2.)

[13] Michaeli, W., Mannigel, M. & Preller, F. 2009 On the effect of shear stresses on the fibre failure behaviour in CFRP. *Composites Science and Technology* **69**(9), 1354-1357. (DOI 10.1016/j.compscitech.2008.09.024.)

[14] Gutkin, R., Pinho, S. T. & Robinson, P. 2011 A finite fracture mechanics formulation to predict fibre kinking and splitting in CFRP under combined longitudinal compression and in-plane shear. *Mechanics of Materials* (accepted for publication).

[15] de Carvalho, N. V., Pinho, S. T. & Robinson, P. 2011 An experimental study of failure initiation and propagation in 2D woven composites under compression. *Composites Science and Technology* **71**(10), 1316-1325. (DOI 10.1016/j.compscitech.2011.04.019.)

[16] de Carvalho, N. V., Pinho, S. T. & Robinson, P. 2011 Numerical Modelling of 2D woven composites: biaxial loading. *Mechanics of Materials* (submitted).

[17] de Carvalho, N. V., Pinho, S. T. & Robinson, P. 2011 Reducing the domain in the mechanical analysis of periodic structures, with application to woven composites. *Composites Science and Technology* **71**(7), 969-979. (DOI 10.1016/j.compscitech.2011.03.001.)

[18] Pinho, S. T., Darvizeh, R., Robinson, P., Schuecker, C. & Camanho, P. P. 2008 Material and structural response of polymer-matrix fibre-reinforced composites. *Composites Science and Technology* (Special issue on Second World Wide Failure Exercise).

[19] de Carvalho, N. V., Pinho, S. T. & Robinson, P. 2011 Analytical modelling of the compressive and tensile response of 2D woven composites. *Composites Part A: Applied Science and Manufacturing* (submitted).
[20] Pinho, S. T., de Carvalho, N. V. & Robinson, P. 2011 Analytical model for the compressive response of 2D woven composites. In *5th International Conference on Composites Testing and Model Identification (CompTest 2011)*. 14-16 February: Ecole Polytechnique Fédérale de Lausanne, Switzerland.
[21] Pimenta, S. & Pinho, S. T. 2011 Recycling carbon fibre reinforced polymers for structural applications: Technology review and market outlook. *Waste Management* **31**(2), 378-392. (DOI DOI: 10.1016/j.wasman.2010.09.019.)
[22] Pimenta, S., Pinho, S. T., Robinson, P., Wong, K. H. & Pickering, S. J. 2010 Mechanical analysis and toughening mechanisms of a multiphase recycled CFRP. *Composites Science and Technology* **70**(12), 1713-1725. (DOI 10.1016/j.compscitech.2010.06.017.)
[23] Pinho, S. T. & Pimenta, S. 2010 The potential of recycled carbon fibres and composites for structural applications. In *Global Outlook for Carbon Fibre 2010*. 29-30 September: IntertechPira, Valencia, Spain.